ADVANCED FUNCTIONAL MATERIALS

Supporting Information

for *Adv. Funct. Mater.*, DOI: 10.1002/adfm.201904858

Charge-Transport Properties of F_6TNAP-Based Charge-Transfer Cocrystals

*Raghunath R. Dasari, Xu Wang, Ren A. Wiscons, Hamna F. Haneef, Ajith Ashokan, Yadong Zhang, Marina S. Fonari, Stephen Barlow, Veaceslav Coropceanu, Tatiana V. Timofeeva, Oana D. Jurchescu, Jean-Luc Brédas, Adam J. Matzger, and Seth R. Marder**

Supporting Information

Charge-Transport Properties of F_6TNAP-based Charge-Transfer Cocrystals

Raghunath R. Dasari,[a] Xu Wang,[b] Ren A. Wiscons,[c] Hamna F. Haneef,[d] Ajith Ashokan,[a] Yadong Zhang,[a] Marina S. Fonari,[b] Stephen Barlow,[a] Veaceslav Coropceanu,[a] Tatiana V. Timofeeva,[b] Oana D. Jurchescu,[c] Jean-Luc Brédas,[a] Adam J. Matzger,[c] Seth R. Marder*[a]

Dr. R. R. Dasari, A. Ashokan,[+] Dr. Y. Zhang, Dr. S. Barlow, Dr. V. Coropceanu, Prof. J.-L Brédas, Prof. S. R. Marder
School of Chemistry and Biochemistry and Center for Organic Photonics and Electronics (COPE)
Georgia Institute of Technology
Atlanta, GA, 30332 USA
E-mail: seth.marder@chemistry.gatech.edu

Dr. X. Wang,[+] Dr. M. S. Fonari, Prof. T. V. Timofeeva
Department of Biology and Chemistry,
New Mexico Highlands University,
Las Vegas, NM, 87701 USA

R. A. Wiscons,[+] Prof. A. J. Matzger
Department of Chemistry and the Macromolecular Science & Engineering Program,
The University of Michigan, Ann Arbor, MI 48109 USA

H. F. Haneef,[+] Prof. O. D. Jurchescu
Department of Physics and Center for Functional Materials,
Wake Forest University, Winston Salem, NC, USA

Dr. M. S. Fonari
Institute of Applied Physics, Chisinau MD-2028, Moldova

[+]These authors made equal contributions.

Contents

I. Donor and Acceptor Energetics

Table S1. Electrochemical potentials[a] and B3LYP/6-31G-calculated orbital energies and adiabatic ionization energy (IE) and electron affinity values (EA) for donor and acceptor molecules.

Molecule	$E_{1/2}^{+/0}$ / V	$E_{1/2}^{0/-}$ / V	E_{HOMO} / eV	E_{LUMO} / eV	IE / eV	EA / eV
TP	+1.10[b]	-	-5.81	-0.78	7.3	–
BTBT	+1.00[c]	-	-5.61	-1.11	7.1	–
BDT	+0.96[b]	-	-5.56	-0.78	7.3	–
PY	+0.94[c]	-	-5.32	-1.37	6.8	–
ANT	+0.88[d]	-	-5.20	-1.53	6.8	–
CBZ	+0.80[d]	-	-5.43	-0.51	7.1	–
F_6TNAP	-	+0.26[e]	-7.32	-5.43	–	4.3

[a] 0.1 M $^nBu_4NPF_6/CH_2Cl_2$ vs $FeCp_2^{+/0}$; [b] peak potential, E_{pa}, from cyclic voltammetry; [c] $E_{1/2}$ from cyclic voltammetry; [d] peak potential from oxidative differential pulse-voltammetry; [e] peak potential from reductive differential pulse-voltammetry

II. Additional Crystallographic Data

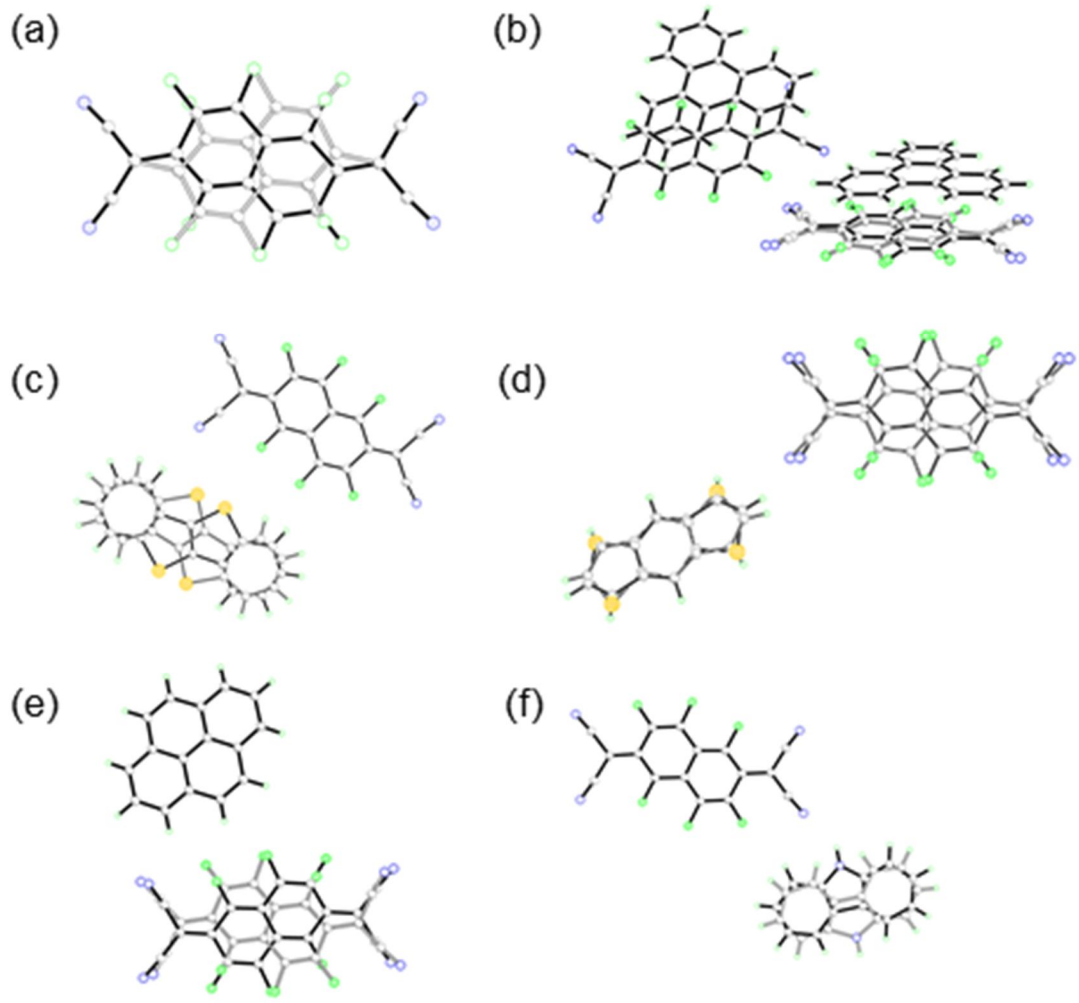

Figure S1. Disorder in Form I of F_6TNAP (a), and in the cocrystals (b) TP:F_6TNAP, (c) BTBT:F_6TNAP, (d) BDT:F_6TNAP, (e) PY:F_6TNAP and (f) CBZ:F_6TNAP.

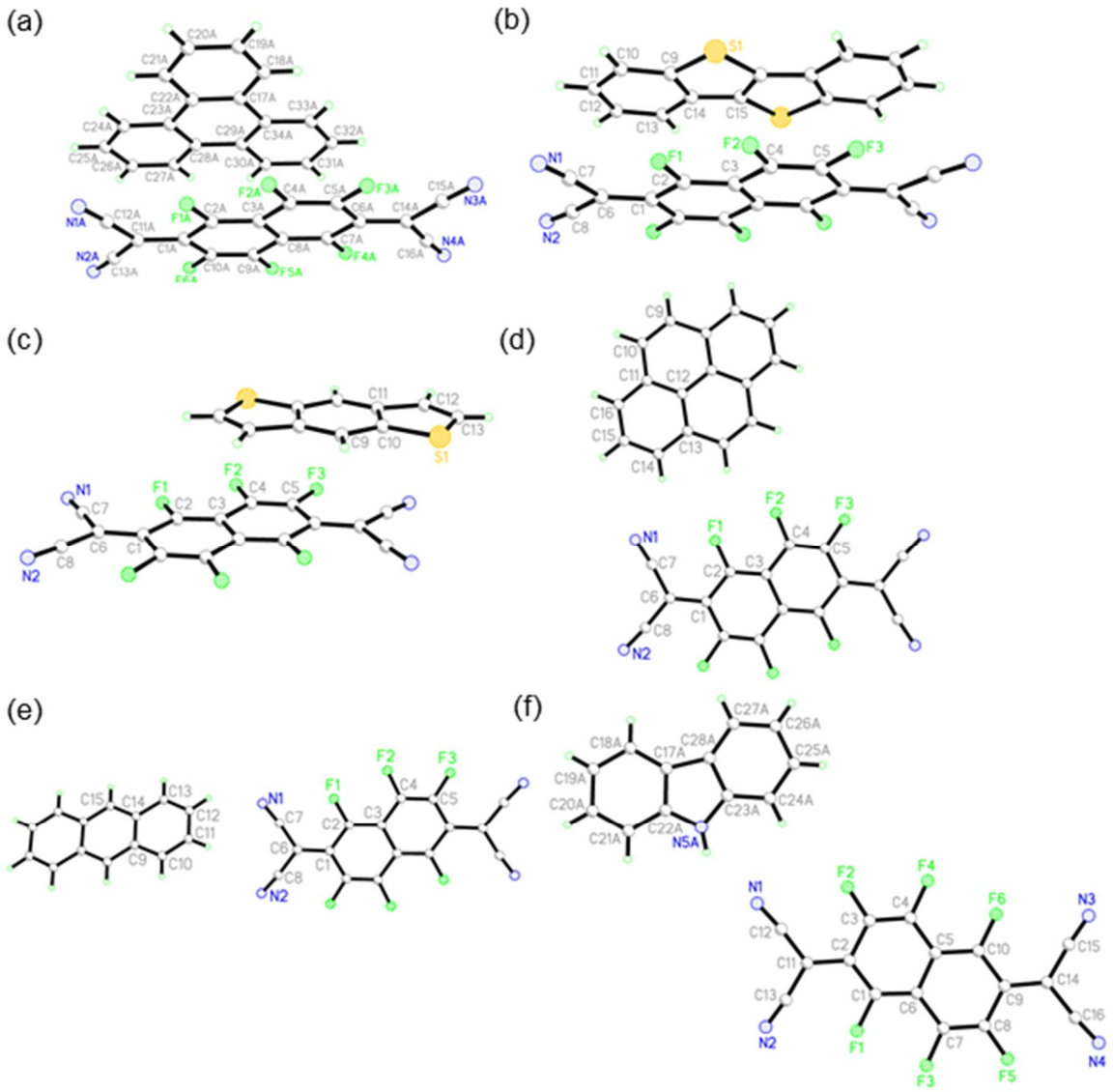

Figure. S2. View of the components in the CT cocrystals: (a) TP:F_6TNAP (only one of two crystallographically unique D:A pairs is shown) (b) BTBT:F_6TNAP (c) BDT:F_6TNAP (d) PY:F_6TNAP (e) ANT:F_6TNAP and (f) CBZ:F_6TNAP with atom numbering schemes.

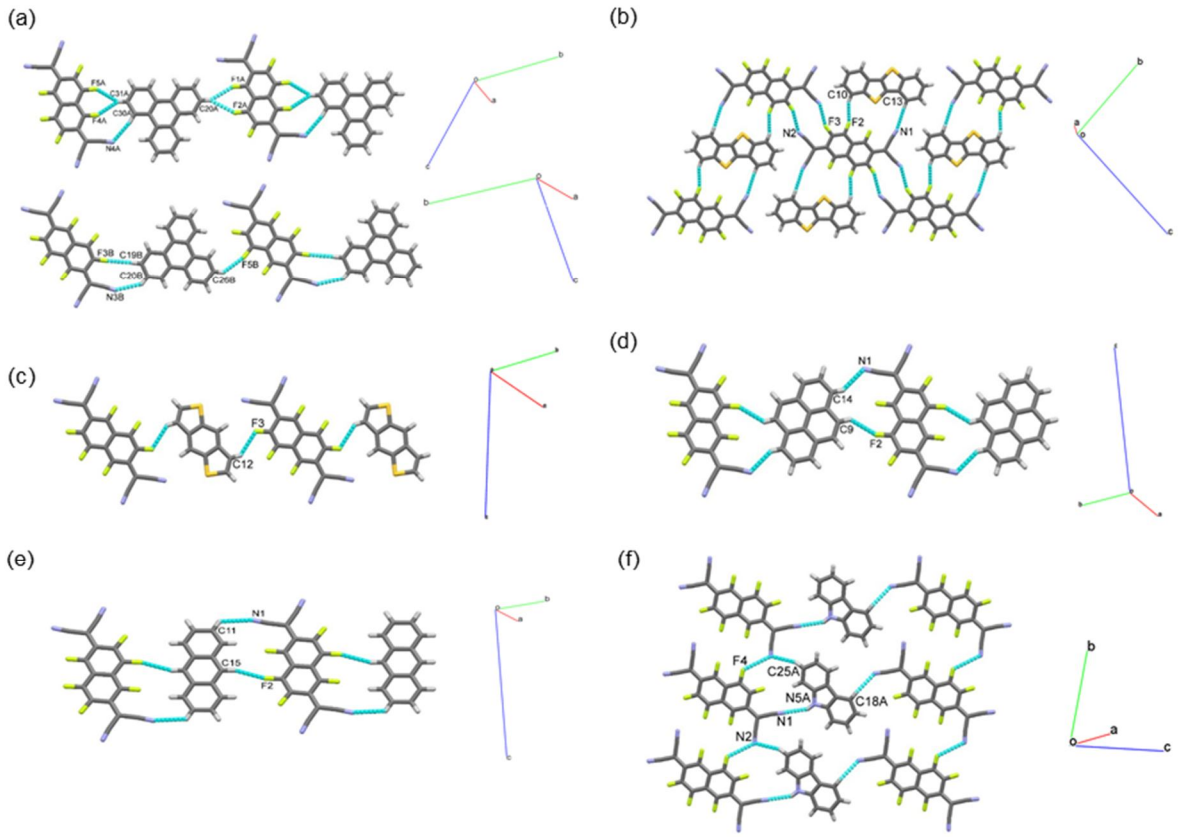

Figure S3. Edge-to-edge contacts that combine the adjacent stacks in the layers in (a) TP:F_6TNAP (a – A and B motifs); (b) BTBT:F_6TNAP; (c) BDT:F_6TNAP; (d) PY:F_6TNAP; (e) ANT:F_6TNAP; and (f) CBZ:F_6TNAP.

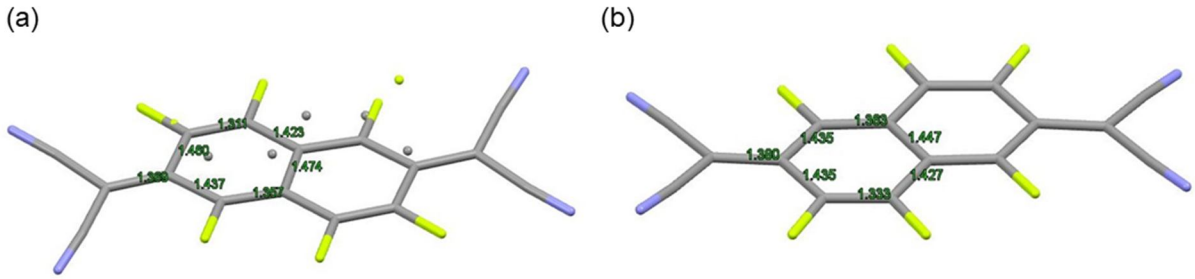

Figure S4. Molecular structure of F_6TNAP in (a) form I and (b) form II with selected bond lengths (in Å) shown.

Table S2. Crystal data and structure refinement parameters.

	F_6TNAP (Form I)	F_6TNAP (Form II)	TP:F_6TNAP	BTBT:F_6TNAP	BDT:F_6TNAP	PY:F_6TNAP	ANT:F_6TNAP	CBZ:F_6TNAP
Empirical formula	$C_{16}F_6N_4$	$C_{12}F_6N_4$	$C_{34}H_{12}F_6N_4$	$C_{30}H_8F_6N_4S_2$	$C_{26}H_6F_6N_4S_2$	$C_{32}H_{10}F_6N_4$	$C_{30}H_{10}F_6N_4$	$C_{28}H_9F_6N_5$
Formula weight	362.20	362.20	590.48	602.52	552.47	564.44	540.42	529.39
Temperature / K	298(3)	298(3)	100(2)	100(2)	100(2)	100(2)	100(2)	298(2)
Crystal system	trigonal	monoclinic	triclinic	triclinic	monoclinic	monoclinic	monoclinic	triclinic
Space Group	$R\bar{3}$	$P2_1/c$	$P\bar{1}$	$P\bar{1}$	$P2_1/n$	$P2_1/c$	$P2_1/c$	$P1$
a / Å	12.6473(10)	6.2926(4)	8.049(2)	6.658(4)	9.410(2)	7.850(3)	7.2487(18)	7.1468(4)
b / Å	17.6473(10)	8.6955(6)	17.369(5)	8.036(5)	7.0084(17)	7.467(3)	6.5963(16)	8.5316(6)
c / Å	11.6795(7)	12.8404(9)	20.139(6)	11.370(7)	16.321(4)	19.834(7)	22.751(6)	9.2592(6)
α / °	90	90	114.669(4)	95.579(9)	90	90	90	81.732(6)
β / °	90	92.708(7)	97.844(4)	99.567(9)	98.179(4)	98.785(5)	93.017(3)	85.619(5)
γ / °	120	90	93.944(4)	102.501(9)	90	90	90	80.033(5)
V / Å^3	3150.0(4)	701.81(8)	2509.5(13)	580.0(7)	1065.4(5)	1148.9(7)	1086.3(5)	549.50(6)
Z	9	2	4	1	2	2	2	1
ρ_{calc} / Mg m^{-3}	1.718	1.714	1.563	1.725	1.722	1.632	1.652	1.600
μ / mm^{-1}	1.462 (Cu Kα)	1.459 (Cu Kα)	0.125 (Mo Kα)	0.311 (Mo Kα)	0.329 (Mo Kα)	0.133 (Mo Kα)	0.136 (Mo Kα)	1.160 (Cu Kα)
F(000)	1602	356	1192	302	552	568	544	266
Crystal size / mm^3	0.05×0.058×0.075	0.075×0.059×0.008	0.40×0.10×0.06	0.30×0.10×0.01	0.50×0.26×0.12	0.292×0.116×0.073	0.497×0.192×0.181	0.087×0.029×0.020
Reflns collected	6220	4237	37082	7630	24840	18155	7963	15379
Indep reflns (R_{int})	1234 (0.0244)	1239 (0.0199)	13907 (0.0354)	2795 (0.0397)	3413 (0.0390)	3877 (0.0356)	3106 (0.0208)	3767 (0.0401)
Data / restr / param	1234 / 0 / 181	1239 / 0 / 118	13907 / 79 / 1028	2795 / 0 / 197	3413 / 14 / 258	3877 / 0 / 230	3106 / 0 / 201	3767 / 3 / 289
GOF (F^2)	1.054	1.077	1.001	1.001	1.050	1.037	1.027	1.053
R indices [$I>2\sigma(I)$] R_1, wR_2	0.0368, 0.1059	0.0349, 0.0983	0.0473, 0.1198	0.0381, 0.0912	0.0429, 0.1274	0.0449, 0.1159	0.0369, 0.1082	0.0591, 0.1517
R indices (all data), R_1, wR_2	0.0406, 0.1095	0.0394, 0.1020	0.0776, 0.1374	0.0527, 0.0973	0.0479, 0.1315	0.0594, 0.1249	0.0375, 0.1119	0.0712, 0.1607

Table S3. C-C bond lengths distribution in the bicyclic core in [Å] of F_6TNAP molecules in cocrystals.[a]

Bond	TP:F_6TNAP(A)	TP:F_6TNAP(B)	Bond	BTBT:F_6TNAP	BDT:F_6TNAP	PY:F_6TNAP	ANT:F_6TNAP	Bond	CBZ:F_6TNAP
C(1)-C(11)	1.391(2)	1.399(4)	C(1)-C(6)	1.373(2)	1.383(2)	1.388(2)	1.386(1)	C(9)-C(14)	1.383(8)
C(6)-C(14)	1.390(2)	1.387(4)						C(2)-C(11)	1.394(9)
C(1)-C(10)	1.439(2)	1.434(4)	C(1)-C(5)#1	1.435(2)	1.432(3)	1.432(2)	1.440(1)	C(8)-C(9)	1.46(1)
C(5)-C(6)	1.441(2)	1.431(5)						C(2)-C(3)	1.46(1)
C(1)-C(2)	1.434(2)	1.430(3)	C(1)-C(2)	1.425(2)	1.429(2)	1.433(2)	1.435(1)	C(9)-C(10)	1.428(9)
C(8)-C(9)	1.433(2)	1.434(3)						C(6)-C(7)	1.429(9)
C(2)-C(3)	1.375(2)	1.371(3)	C(2)-C(3)	1.368(2)	1.365(2)	1.372(2)	1.372(1)	C(5)-C(10)	1.412(8)
C(9)-C(10)	1.348(2)	1.338(4)						C(7)-C(8)	1.347(6)
C(3)-C(4)	1.433(2)	1.431(3)	C(3)-C(4)	1.427(2)	1.430(2)	1.432(2)	1.434(1)	C(1)-C(2)	1.39(1)
C(6)-C(7)	1.433(2)	1.431(3)						C(4)-C(5)	1.41(1)
C(3)-C(8)	1.446(2)	1.447(3)	C(3)-C(3)#1	1.441(3)	1.438(3)	1.444(2)	1.446(2)	C(5)-C(6)	1.452(9)
C(4)-C(5)	1.351(2)	1.347(5)	C(4)-C(5)	1.337(2)	1.337(3)	1.345(2)	1.350(1)	C(3)-C(4)	1.349(9)
C(7)-C(8)	1.372(2)	1.370(3)						C(1)-C(6)	1.361(8)

Note: * Symmetry transformation \$1: *-x*, 2-*y*, 1-*z* in PY:F_6TNAP; *–x*, 1-*y*, *-z* in ANT:F_6TNAP; 2*–x*, 2-*y*, *-z* in BDT:F_6TNAP; 1*–x*, *-y*, *-z* in BTBT:F_6TNAP; [a] See Figure 3 for atom numbering; values in parentheses are standard deviations.

Table S4. Shortest intermolecular contacts in the cocrystal structures.

Crystal	Type of interaction	Contact	d(D-H…A; H…A) (Å); ∠DHA (°)	Acceptor symmetry transformation
TP:F_6TNAP	Edge-to-edge D…A contacts between adjacent stacks in layers	C(20A)-H(20A)…F(1A)	2.58(3); 3.431(3); 145(2)	1-x, -y, 1-z
		C(20A)-H(20A)…F(2A)	2.66(2); 3.522(2); 153(2)	1-x, -y, 1-z
		C(30A)-H(30A)…N(4A)	2.67(2); 3.575(3); 160(1)	2-x, 1-y, 1-z
		C(31A)-H(31A)…F(4A)	2.51(2); 3.292(2); 136(1)	2-x, 1-y, 1-z
		C(31A)-H(31A)…F(5A)	2.58(2); 3.374(2); 141(1)	2-x, 1-y, 1-z
		C(26B)-H(26B)….F(5B)	2.52(2); 3.264(5); 133(2)	-x, 1-y, -z
		C(20B)-H(20B)…N(3B)	2.67(2); 3.421(5); 137(1)	1-x, -y, -z
		C(19B)-H(19B)…F(3B)	2.48(2); 3.413(3); 166(1)	1-x, -y, -z
	Edge-to-edge D(A,B)...A(B,A) leading to herring-bone packing	C(18A)-H(18A)…N(13B)	2.56(2); 3.497(7); 163(2)	1+x, y, 1+z
		C(24A)-H(24A)…N(1B)	2.63(2); 3.552(7); 165(2)	-x, -y, -z
		C(25A)-H(25A)…N(3B)	2.61(2); 3.298(5); 129(1);	x-1, y, z
		C(33A)-H(33A)…N(2B)	2.42(2); 3.333(8); 160(1)	1+x, y, 1+z
		C(18B)-H(18B)…N(2A)	2.57(2); 3.488(2); 163(1)	x, y, z
		C(21B)-H(21B)…N(1A)	2.59(2); 3.525(2) 165(1)	–x, -y, -z
		C(24B)-H(24B)…N(1A)	2.57(1); 3.495(2) 162(1)	–x, -y, -z
BTBT:F_6TNAP	Edge-to-edge D...A contacts (all in-layer)	C(13)-H(13)…N(1)	2.731; 3.585(3); 150.00	x-1, y-2, z
		C(10)-H(10)….F(2)	2.488; 3.277(2); 140.5	1-x, 2-y, -z
	A-A contacts	C(5)-F(3)…N(2)	2.968(2); 131.4	x, y, z-1
		C(4)-F(2)…N(1)	3.002(2); 111.2	1-x, 3-y, -z
BDT:F_6TNAP	D...A side contacts within the layer	C(12)-H(12)…F(3)	2.67; 3.42(1); 136.8	1-x, 1-y, -z
	A…A side contacts in the layer	C(4)-F2…F(2)	2.898(2); 86.89	2-x, 1-y, -z

	D…A side contacts between layers	C(13)-H(13A)...N(1)	2.493; 3.356(7); 151.02	x-3/2, 3/2-y, z-1/2
PY:F_6TNAP	Edge-to-edge D…A between adjacent stacks in the layers.	C(14)-H(14)…N(1)	2.60(2); 3.393(2); 143(1)	x, y, z
		C(9)-H(9)…F(2)	2.53(2); 3.293(2); 135(1)	1-x, -y, 1-z
	Edge-to-edge D...A contacts leading to herring-bone packing	C(10)-H(10)…N(2)	2.64(2); 3.613(2); 160.6	1-x, y-1.5, 0.5-z
		C(15)-H(15)…N(1)	2.66(2); 3.333(2); 120.93	1-x, y-0.5; 0.5-z
ANT:F_6TNAP	Edge-to-edge D…A contacts between adjacent stacks in layers	C(11)-H(11)…N(1)	2.70(2); 3.325(2) 122(1)	1-x, y-0.5, 0.5-z
		C(15)-H(15)…F(2)	2.61(1); 3.443(1); 149(1)	1-x, 0.5+y, 0.5-z
	A…A-in the layer	C(2)-F(1)…F(2)	2.846(1); 100.6(1)	-x, 2-y, -z
		C(4)-F(2)…F(2)	2.841(1); 99.2(1)	-x, 2-y, -z
	Edge-to-edge D...A contacts leading to herring-bone packing	C(12)-H(12)…N(1)	2.57(1); 3.337(1); 133(1)	x,y,z
		C(12)-H(12)…N(2)	2.58(2); 3.367(2); 135(1)	x, 1+y, z
CBZ:F_6TNAP	Edge-to-edge D...A contacts (all in-layer)	N(5A)-H(5A)…N(1)	2.37; 3.10(1); 143.6	x, y, z
		C(25A)-H(25A)…N(2)	2.62; 3.47(1); 152.2	x, 1+y, z
		C(18A)-H(18A)…N(4)	2.60; 3.48(1); 159.9	1+x, y, 2+z
		C(4)-F(4)…N(2)	3.01(1); 3.95(1); 125.3(4)	x, 1+y, z

III. Infrared Data

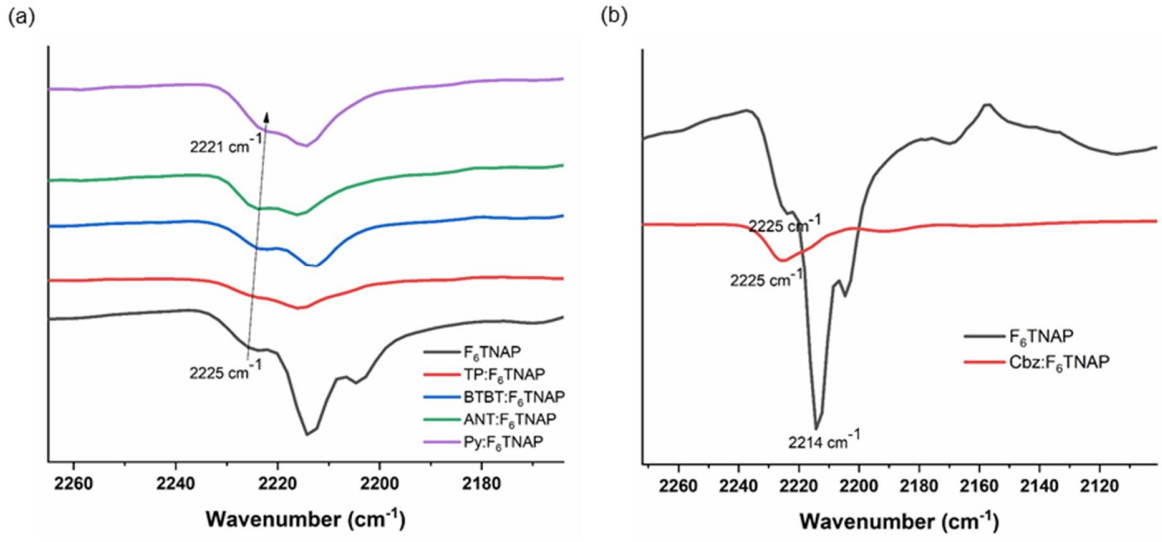

Figure S5. IR spectra comapring the nitrile stretching modes of F_6TNAP with (a) TP:F_6TNAP, BTBT:F_6TNAP, ANT:F_6TNAP, PY:F_6TNAP cocrystals, and (b) CBZ:F_6TNAP.

Table S5. Highest nitrile strecthing frequencies (cm^{-1}) for F_6TNAP, cocrystals, and $F_6TNAP^{\bullet-}$, ν_0, ν_{CT}, and ν_1, respectively, and along with estimated degree of charge transfer (ρ) for cocrystals.[a]

Cocrystal	ν_0	ν_{CT}	ν_1	ρ
TP:F_6TNAP	2225	2223	2194	0.06±0.03
BTBT:F_6TNAP	2225	2222	2194	0.09±0.03
BDT:F_6TNAP	2225	2223	2194	0.06±0.03
PY:F_6TNAP	2225	2221	2194	0.13±0.03
ANT:F_6TNAP	2225	2223	2194	0.06±0.03

[a] Estimated using eq. 1.

IV. Additional DFT Electronic Structure Data

(a)

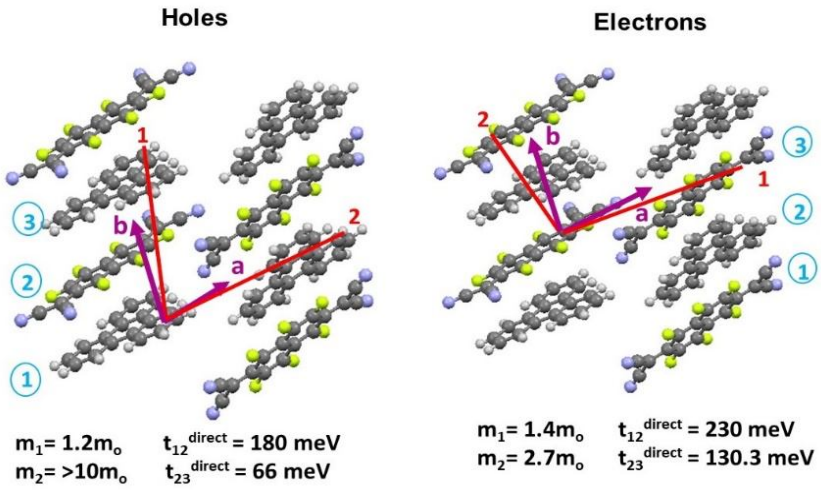

(b)

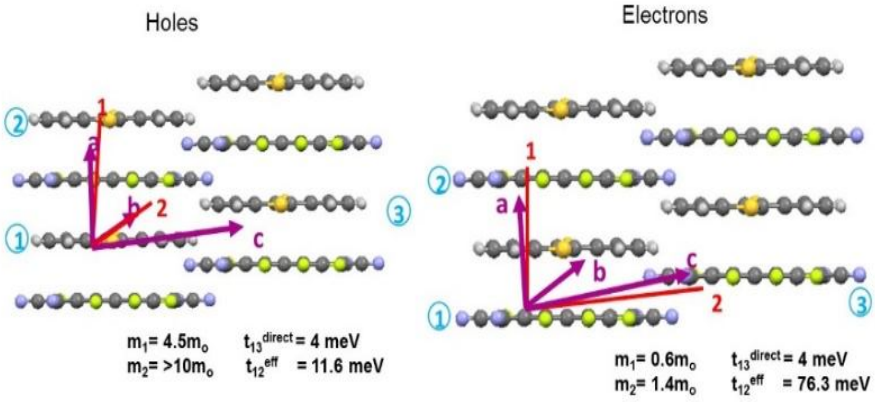

(c)

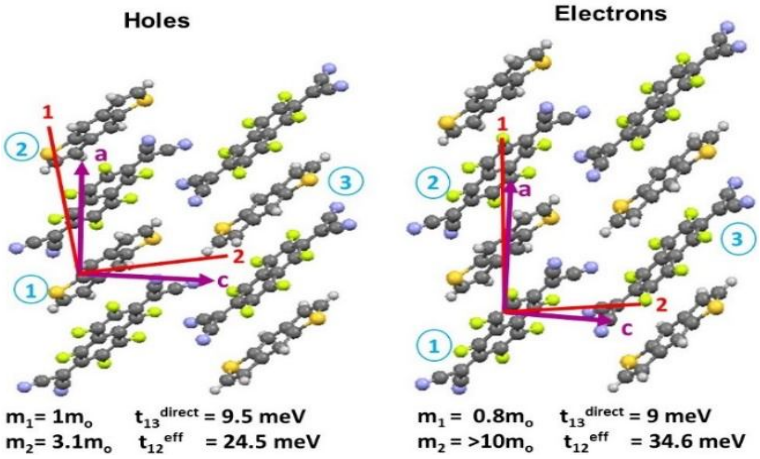

(d)

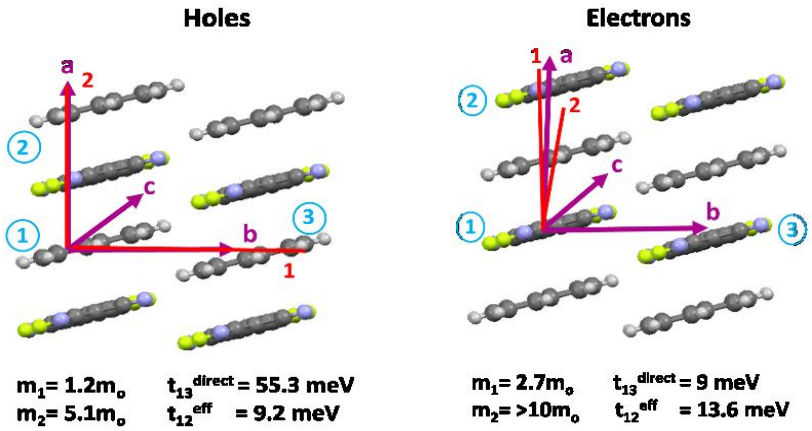

(e)

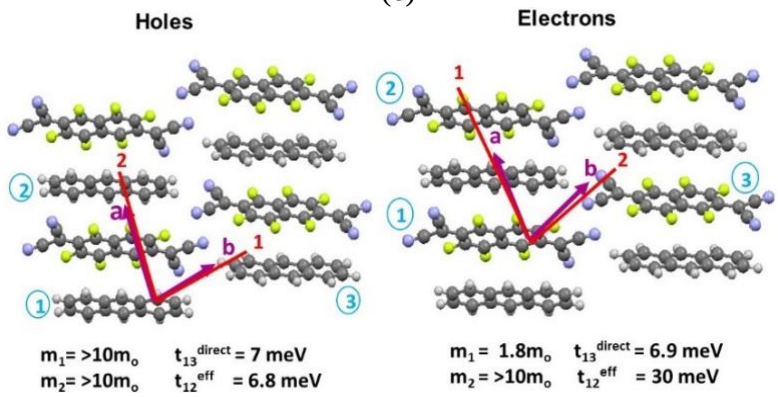

(f)

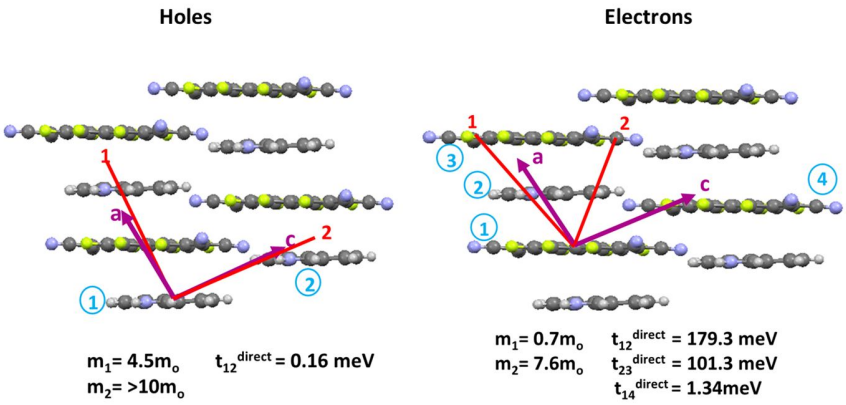

Figure S6. Illustrations of the largest transfer integrals and smallest effective masses for holes and electrons in the structures of (a) TP:F_6TNAP, (b) BTBT:F_6TNAP, (c) BDT:F_6TNAP, (d) PY:F_6TNAP; (e) ANT:F_6TNAP, and (f) CBZ:F_6TNAP. The red lines indicate the directions along which the principal components of m_{ji}^{-1} have the smallest values of the effective mass.

Table S6. B3LYP/6-31G estimates of E_{DA} (copmuted using the IP and EA values from Table S1), t_{DA} and super-exchange couplings for holes (t_h^{eff}) and electrons (t_e^{eff}).

Co-crystals	E_{DA} (eV)	t_{DA} (meV)	t_h^{eff} (meV)	t_e^{eff} (meV)
TP:F6TNAP	3.0	185.4/66 230/130.3	-	-
BTBT:F6TNAP	2.8	300.5	11.6	76.3
BDT:F6TNAP	3.0	163.5	24.5	34.6
PY:F6TNAP	2.5	186.4	9.2	13.6
ANT:F6TNAP	2.5	125.3	6.8	30
CBZ:F6TNAP	2.8	179.3/101.3	-	-

Table S7. Hole and electron effective masses, *m* (in units of the free electron mass at rest, m_0).

Crystal		m / m_0	Parallel to
TP:F_6TNAP	Holes at X (0.5, 0, 0)	1.2	b+0.35a+0.005c
		10.77	a-0.05b-0.017c
		1129.9	c+0.49a+0.48b
	Electrons at R(0.5, 0.5, 0.5)	1.4	a+0.13b+0.23c
		2.7	b-0.81a+0.97c
		4.9	b+0.49a-0.46c
BTBT:F_6TNAP	Holes at U (0.5, 0, 0.5)	4.5	a-0.27b-0.03c
		11.4	b+0.7a+0.36c
		107.8	c-0.02a-0.54c
	Electrons at X (0.5,0,0)	0.64	a+0.29b+0.31c
		1.40	c+0.77b-0.77a
		171.9	b+0.1a-0.33c
BDT:F_6TNAP	Holes at Γ (0, 0, 0)	1.01	a+0.2c
		3.06	c-0.37a
		20.0	b
	Electrons at Z (0, 0.5, 0)	0.81	a+0.006c
		18.5	b+0.2a
		30.0	b
PY:F_6TNAP	Holes at Γ (0, 0, 0)	1.25	b
		5.01	a+0.04c
		35.13	c+0.078a
	Electrons at (0, 0.2, 0)	2.76	a+0.36c
		10.13	a-0.43c
		120	b
ANT:F_6TNAP	Holes at E (-0.5, 0.5, 0.5)	17.1	b
		468.6	a-0.6c
		158.7	a+0.18c

	Electrons at D (0, 0.5, 0.5)	1.81	a+0.0002c
		12.4	b
		240.1	c+0.16a
CBZ:F_6TNAP	Holes at Γ (0, 0, 0)	4.56	a-0.05b
		60.00	c-0.06a-0.14b
		70.77	b-0.13a
	Electrons at (0, 0.035, 0.5)	0.75	a-0.24b+0.25c
		7.61	c-0.45a+0.22b
		60.83	b+0.19a-0.22c

IV. Additional Electrical Characterization

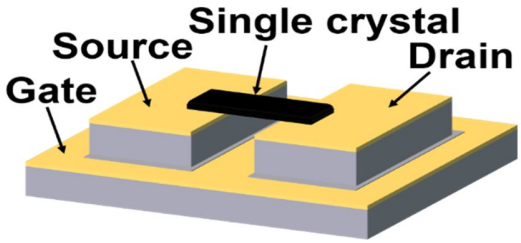

Figure S7. Device geometry for electrical characterization. SCLC measurements were ungated, whereas for OFETs a gate electrode was used.

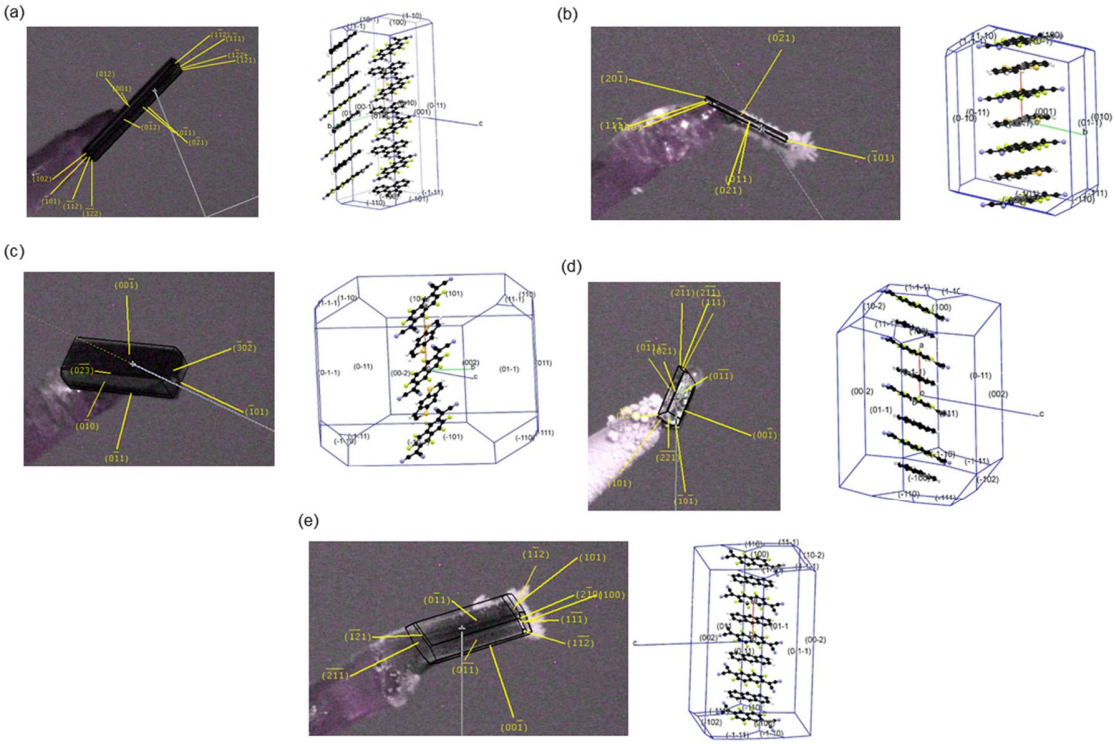

Figure S8. Observed and simulated (using the Mercury program) morphology of (a) TP:F_6TNAP, (b) BTBT:F_6TNAP, (c) BDT:F_6TNAP, (d) PY:F_6TNAP, and (e) ANT:F_6TNAP cocrystals.

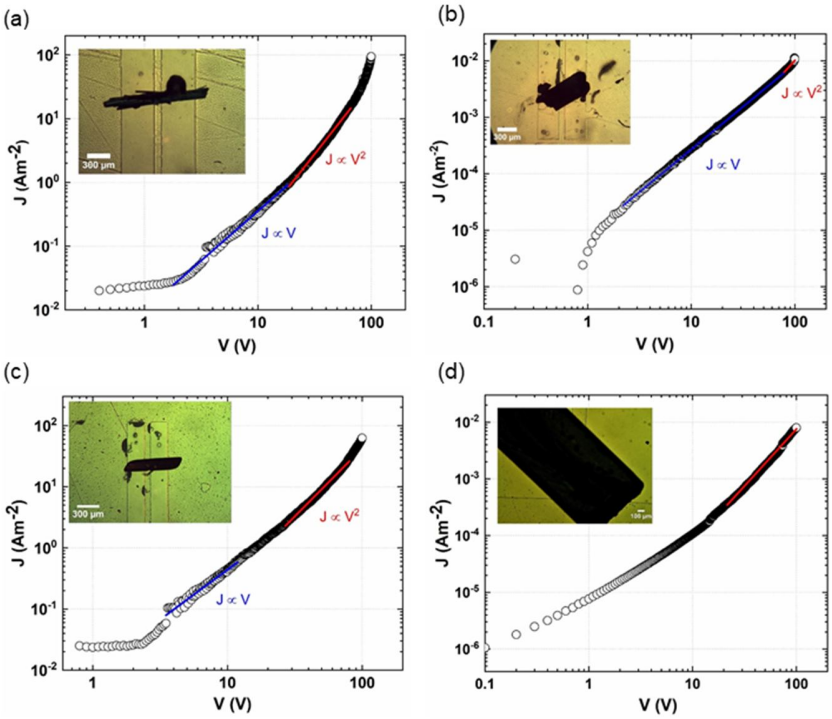

Figure S9. SCLC current-voltage curves of a) TP:F_6TNAP, b) BDT:F_6TNAP, c) PY:F_6TNAP, d) ANT:F_6TNAP cocrystals. Insets on each graph show an optical micrograph of the corresponding crystal laminated across the electrodes. The blue and red solid lines represent linear fits for the ohmic and SCLC regimes respectively.

Table S8. Summary of dimensions (µm) used in SCLC measurements along with the electrical properties obtained.

Crystal	length	width	thickness	μ_{SCLC} / $cm^2 V^{-1} s^{-1}$	ρ / Ω m
TP:F_6TNAP	80	169	70	0.56 ± 0.07	2.0×10^5
BTBT:F_6TNAP	80	214	10	1.1 ± 0.36	2.0×10^5
BDT:F_6TNAP	80	380	120	$(2.3 \pm 0.32) \times 10^{-4}$	5.1×10^8
ANT:F_6TNAP	200	1200	500	$(2.0 \pm 0.14) \times 10^{-3}$	4.7×10^8
CBZ:F_6TNAP	80	38	10	9.0 ± 0.61	5.2×10^3
PY:F_6TNAP	80	152	75	0.62 ± 0.04	2.3×10^5

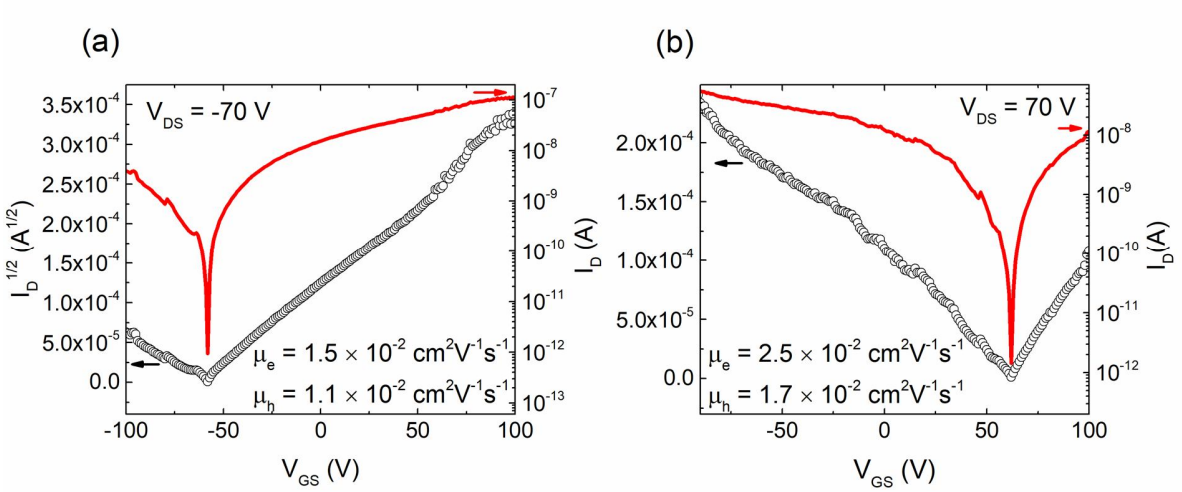

Figure S10. Evolution of the drain current, I_D as a function of the gate-source voltage, V_{GS} for the PY:F_6TNAP cocrystal at a) V_{DS} = -70 V and b) V_{DS} = 70 V. The left axis shows the square root of I_D while the right axis shows a log-scale plot of I_D. The reliability factor for the graph in panel (a) is 97%, and for the graph in panel (b) 70%.

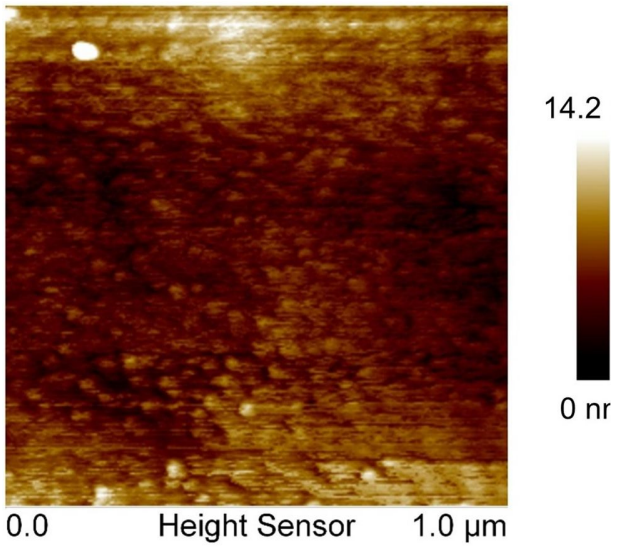

Figure S11. Atomic force microscopy image of a PY:F_6TNAP crystal face showing roughness of a PY:F_6TNAP cocrystal.